World Scientific
www.worldscientific.com

INVESTIGATION OF INCOMPLETE FUSION IN ^{19}F + ^{159}Tb REACTION AT BEAM ENERGY OF ~ 5 MeV/NUCLEON

AMIT KUMAR, K. SUDARSHAN*, SUPARNA SODAYE,
R. TRIPATHI and P. K. PUJARI

Radiochemistry Division, Bhabha Atomic Research Centre,
Trombay, Mumbai 400 085, India
*kathis@barc.gov.in

Formation cross-sections of evaporation residues have been measured in ^{19}F + ^{159}Tb reaction at E_{lab} = 83, 88, 93, 98 and 103 MeV using recoil catcher technique followed by off-line gamma-ray spectrometry. Significant contribution from incomplete fusion has been observed at these low beam energies indicating the contribution to incomplete fusion from collision trajectories with angular momentum (l) less than the critical angular momentum for complete fusion (l_{cr}(CF)). Incomplete fusion cross-sections could be explained using a modified sum-rule model which allows effective competition from incomplete fusion for collision trajectories with $l < l_{\text{cr}}$(CF).

Keywords: Incomplete fusion; recoil catcher technique; gamma-ray spectrometry.

1. Introduction

Heavy ion fusion has been one of the most widely investigated subjects in the area of low and intermediate energy heavy ion reactions. Such studies have helped in understanding the various processes occurring during the collision of nuclei such as quasi-elastic transfer (QET), incomplete fusion reactions (ICF), and deep inelastic collisions (DIC). Contribution from these different types of reactions depends on the beam energy and projectile–target combination. QET reactions involve transfer of a few nucleons and the spectra of corresponding projectile like fragments are peaked around optimum Q value, i.e. Q_{opt}.[1] Dissipative effects are minimal in QET reactions. On the other hand, DIC reaction involves large kinetic energy dissipation, manifested as low energy tail in the kinetic energy spectra of projectile like fragments (PLFs) extending up to the exit channel Coulomb energy. In DIC, projectile and target stick together for sufficiently long time so that there is an exchange of significant number of nucleons between the projectile and the target nuclei. Incomplete fusion reactions are expected to lie between QET and DIC in terms of kinetic energy dissipation. In ICF,[2,3] a part of the projectile fuses with the target and other continues to move in the forward direction with approximately

beam velocity. Transfer of mass takes place from the lighter reaction partner (usually projectile) to the heavier one in ICF reactions. Angular distributions of PLFs formed in ICF are forward peaked compared to those of PLFs formed in QET.[4,5] In our earlier studies, it was observed that the cross-section of lighter PLFs formed in incomplete fusion or massive transfer reaction falls more rapidly with decreasing beam energy compared to those of heavier PLFs formed in the transfer of a few nucleons.[6,7] This observation suggested significant overlap of the projectile and target nuclei in incomplete fusion reactions. Such collision trajectories would lead to incomplete fusion at higher beam energies due to the large angular momentum, which would otherwise lead to complete fusion at lower beam energies. Deeper interpenetration of the projectile and target nuclei in incomplete fusion reactions has been reported in earlier studies.[8–10] Measurements on gamma-ray multiplicity in coincidence with outgoing PLFs have indicated the localization of ICF channels in angular momentum window extending below the critical angular momentum for complete fusion ($l_{cr}(CF)$).[8–10] Measurement of spin distribution of evaporation residues by Singh *et al.* in $^{16}O + {}^{169}Tm$ reaction showed localization of incomplete fusion close to the critical angular momentum for complete fusion.[11]

Several models, namely, break-up fusion models by Udgawa and Tamura,[12] promptly emitted particle (PEP) model by Bondorf *et al.*,[13] Exciton model by Blann,[14] multi-step direct reaction theory by Zagrebaev[15] and sum-rule model by Wilczynski *et al.*[1,16] were proposed to explain incomplete fusion reactions. Morgenstern *et al.*[17,18] showed a correlation between the probability of ICF reaction and entrance channel mass asymmetry. Projectile structure also plays an important role in incomplete fusion reactions. Most of the studies involving projectiles with alpha cluster structure e.g. ^{12}C (Refs. 19–26), ^{16}O (Refs. 26–32), ^{24}Mg (Ref. 33) and ^{20}Ne (Ref. 34) have shown significant contribution from ICF reactions. Sum-rule model,[1,16] which allows effective competition from ICF only for collision trajectories with $l > l_{cr}(CF)$, successfully explains the ICF cross-section at higher beam energies ($\sim > 10$ MeV/nucleon), however, it underestimates the ICF cross-section at lower beam energies (~ 5 MeV/nucleon). At lower beam energies, it is necessary to consider the contribution from low l-waves to ICF to explain experimentally observed ICF cross-section.[7] These observations suggest that reactions involving incomplete mass transfer are not well understood and, therefore, heavy ion fusion continue to be an active area of investigation.[19–35]

In the present work, cross-sections of evaporation residues (ERs) for complete and incomplete fusion channels have been measured in $^{19}F + {}^{159}Tb$ reaction in the beam energy range 83–103 MeV to investigate incomplete fusion reactions at lower beam energies (~ 5 MeV/A). cross-sections have been measured by radiochemical method which involves recoil catcher technique followed by off-line gamma-ray spectrometry. Experimental cross-sections have been compared with the calculations of statistical model code PACE2[36] to investigate the contribution from ICF. Results of the calculation using sum-rule model[1] and modified sum-rule model,[7]

which allow competition from ICF for collision trajectories with $l < l_{\mathrm{cr}}(\mathrm{CF})$ are also presented.

2. Experimental Methods

Experiments were carried out at Pelletron-LINAC facility at Tata Institute of Fundamental Research, Mumbai, India. Self-supporting targets of ^{159}Tb metal foil (thickness ~ 2 mg/cm^2) were bombarded with ^{19}F beam. A super-pure aluminum catcher foil (~ 6.75 mg/cm^2) was kept in the forward direction to stop the evaporation residues recoiling out of the target. Irradiations were carried out at $E_{\mathrm{lab}} = 83$, 88, 93, 98 and 103 MeV. At each beam energy, one long irradiation ($T_{\mathrm{irr}} \sim 5$–6 h) was carried out. In addition, at $E_{\mathrm{lab}} = 93$, 98 and 103 MeV, short irradiation

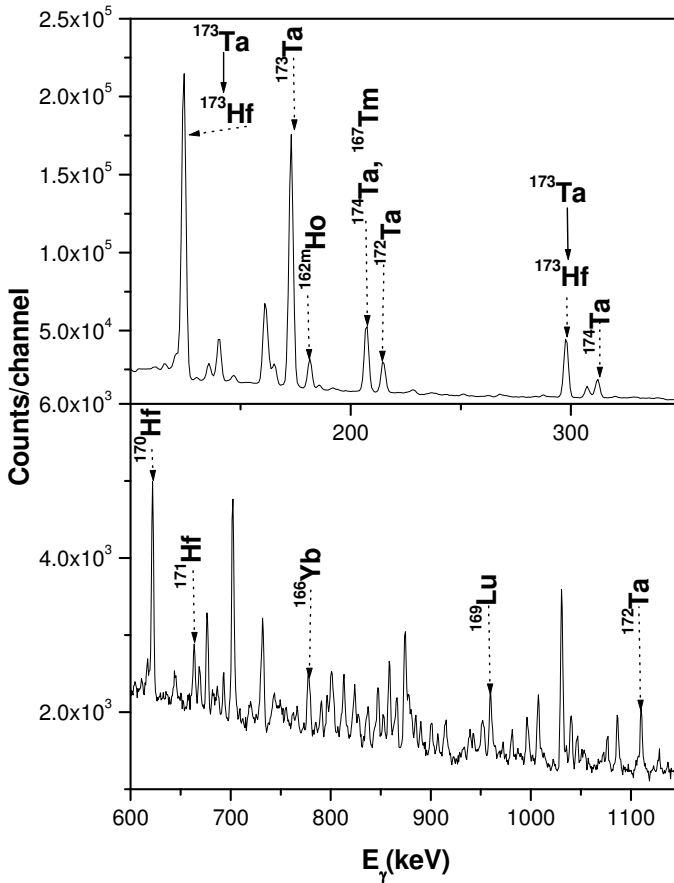Fig. 1. Typical gamma-ray spectra (top panel: $E_\gamma = 100-350$ keV; bottom panel: 600–1150 keV) of evaporation residues (ERs) produced in ^{19}F + ^{159}Tb reaction at beam energy of 103 MeV, $T_{\mathrm{cool}} = 111$ min, counting time = 3000 sec. Gamma-rays from different ERs are marked in the figure.

Table 1.   Nuclear data used in the present study for the calculation of cross-sections of various evaporation residues (ERs) taken from Ref. 37. The reaction channels for the formation of evaporation residues shown in this table may involve emission of different ejectiles, therefore various reaction channels are expressed in terms of protons and neutrons as ejectiles.

S1. No.	Radio nuclide	Half-life	E_γ (kEV)	Abundance (%)	Channel
1	^{174}Ta	1.14 h	206.5, 310.9, 764.8, 1206.9	60.0, 1.25, 1.26, 4.9	(^{19}F, $4n$) and EC/β^+ decay or (^{19}F, $p3n$)
2	^{173}Ta	3.14 h	172.2, 180.6	17.5, 2.1	(^{19}F, $5n$) and EC/β^+ decay or (^{19}F, $p4n$)
3	^{172}Ta	36.8 min	214.07, 1109.3	55, 14.9	(^{19}F, $6n$) and EC/β^+ decay or (^{19}F, $p5n$)
4	^{171}Hf	12.1 h	662.0	14.8	(^{19}F, $2p5n$)
5	^{170}Hf	16.01 h	164.7, 620.7	33.5, 22.9	(^{19}F, $2p6n$)
6	^{169}Lu	34.06 h	191.2, 960.6	18.7, 21.2	(^{19}F, $3p6n$)
7	^{167}Yb	17.5 min	113.3, 176.2	55, 20.4	(^{19}F, $4p7n$)
8	^{166}Yb	2.36 days	778.8	24.9	(^{19}F, $4p8n$)
9	^{167}Tm	9.25 days	207.8	42	(^{19}F, $5p6n$)
10	^{162m}Ho	68.0 min	186.0	29.2	(^{19}F, $7p9n$)
11	^{161m}Ho	2.48 h	103.5	3.9	(^{19}F, $7p10n$)

($T_{\rm irr} \sim 1$ h) was also carried out. During the irradiation, beam current was monitored using an electron suppressed Faraday cup, placed behind the target catcher assembly. Current from the Faraday cup was recorded through a current integrator every 30 sec. This allowed minimizing the error in the cross-section measurement of shortlived radionuclides due to the fluctuation in the beam intensity. After irradiation, gamma-ray activity in the target and catcher foil together was measured using a pre-calibrated 30% relative efficiency HPGe detector coupled to a 4 K multichannel analyzer. Typical gamma-ray spectra of ERs produced in ^{19}F + ^{159}Tb reaction at beam energy of 103 MeV is shown in Fig. 1. In the gamma-ray spectra, peaks due to the characteristic gamma-rays of different evaporation residues were identified, which are marked in the figure. Assignment of gamma-rays was further confirmed by following the decay of the evaporation residues. Nuclear data required for the identification of the evaporation residues and determination of their formation cross-sections were taken from Ref. 37. Gamma-ray spectra of the evaporation residues were analyzed using the peak area analysis software PHAST[38] developed at Bhabha Atomic Research Centre, Mumbai. From the peak areas, end of irradiation activity of an evaporation residue (A) was determined using the equation

$$A = \frac{PA\dfrac{\rm CT}{\rm LT}}{e^{-\lambda T_{\rm cool}}[(1 - e^{-\lambda {\rm CT}})/\lambda](I_\gamma/100)\varepsilon} \qquad (1)$$

where, LT is the live time of analog to digital converter (ADC) and CT is the corresponding clock time. First term in the denominator is a correction factor for the decay during the time $T_{\rm cool}$, elapsed from the end of irradiation to the start of counting. Second term in the denominator is a correction factor for the decay during

counting time CT. I_γ is the percentage gamma-ray intensity taken from Ref. 37 and ε is the full energy detection efficiency of the HPGe detector. The HPGe detector was efficiency calibrated using ^{152}Eu^g and ^{133}Ba^g standard sources. From the end of irradiation activity A of an evaporation residue, its formation cross-section (σ) was calculated using the equation

$$\sigma = \frac{A}{N \sum_{i=1}^{n} \phi_i (1 - e^{-\lambda \Delta T_{\mathrm{irr}}}) e^{-\lambda(T_{\mathrm{irr}} - i \Delta T_{\mathrm{irr}})}} \qquad (2)$$

where, N is the number of target atoms per unit area, λ is the decay constant, T_{irr} is the total irradiation time, n is the number of intervals and ΔT_{irr} (= 30 sec) is the time interval for which average current was recorded. Decay data[37] of evaporation residues used in the calculation of their formation cross-section is given in Table 1. Reaction channels for the formation of evaporation residues are also given in this table. A given reaction channel may involve emission of different ejectiles, therefore various reaction channels are expressed in terms of protons and neutrons as ejectiles.

3. Results and Discussion

Tungsten (W) isotopes formed in the complete fusion reaction are short lived and decay to Ta isotopes. Fitting of γ-ray activity of Ta isotopes using decay-growth equation did not show any significant contribution from direct formation of Ta isotopes, therefore formation cross-section of Ta isotope was attributed to the corresponding W isotope. The excitation function of ERs formed in complete and incomplete fusion channels in ^{19}F+^{159}Tb reaction are shown in Figs. 2(a)–(f). The experimental cross-sections are shown as solid symbols. The uncertainties shown in Fig. 2 are due to the counting statistics and peak-fitting. Tungsten isotopes correspond to complete fusion channel, Hf isotopes correspond to (^{19}F, $2pxn$) channel, Lu isotopes correspond to (^{19}F, $3pxn$) channel, Yb isotopes correspond to (^{19}F, $4pxn$) channel, Tm isotopes correspond to (^{19}F, $5pxn$) channel, and Ho isotopes correspond to (^{19}F, $7pxn$) channel. Cross-sections for (^{19}F, $6pxn$) channel could not be measured as most of the Er isotopes formed in the reaction were either very short lived or having no gamma rays. Similarly, cross-sections for the ERs formed following emission of PLFs with $Z = 8$ could not be measured due to the unsuitable decay characteristics of the evaporation residues. However, it would not affect the results of the present study which is mainly focused towards investigation of incomplete or massive transfer reactions involving large mass transfer.

In order to estimate the contribution from ICF reactions, cross-section for evaporation residues were calculated using the statistical model code PACE2.[36] The RKK level density prescription[39] was used in PACE2 calculations. PACE2 gives the probabilities of statistical de-excitation of the compound nucleus to different decay channels. Statistical decay probabilities are converted to cross-section using angular momentum distribution (l) of the compound nucleus. The l distribution
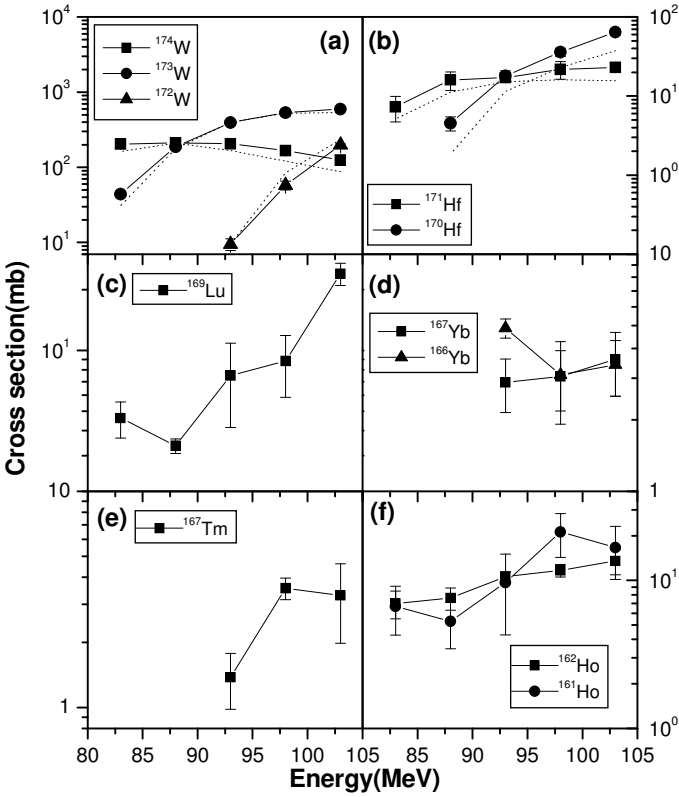
Fig. 2.   Theoretical and experimental excitation function of evaporation residues (ERs) produced in ^{19}F + ^{159}Tb reaction. Solid lines are eye guides to the experimental data and dashed lines represent cross-sections calculated using PACE2.[36]

of compound nucleus was generated using CCFUS[40] and was given as input to PACE2. The parameters of PACE2 code were fixed by reproducing the experimental cross-sections of W isotopes which are formed in complete fusion. The level density parameter "a" was fixed at $A/9.0$ MeV^{-1} and yrast line was multiplied by a factor of 1.4. The results of PACE2 calculations are shown as dotted lines in Figs. [2(a) and (b)].

It can be seen from Fig. 2(b) that the experimental cross-sections of Hf isotopes formed in (^{19}F, $2pxn$) channel are significantly higher as compared to the calculations of PACE2. Larger experimental cross-sections for Hf isotopes indicate the contribution from ICF reaction in the formation of these isotopes. The lighter evaporation residues, namely, Lu–Ho isotopes are expected to be predominantly formed in ICF reaction. According to the calculations of the code PACE2, the upper limit of the CF contribution to the experimental cross-sections of Lu, Yb, Tm and Ho isotopes was 7.5%. For the cases where model calculations did not predict any cross-section, CF contributions were estimated based on the lowest cross-sections,

obtained in the present calculations with the statistical uncertainty of 10%. ICF cross-sections were estimated from experimental cross-section of Hf and lighter isotopes after correcting for CF contribution to Hf isotopes using the calculation of PACE2. Also, the experimental cross-sections of ^{169}Lu were corrected for the contribution due to the decay of ^{169}Hf, formed in CF, using PACE2 calculations. Total ICF cross-sections, obtained by adding incomplete fusion contribution to different ERs, were 13 ± 4, 23 ± 5, 50 ± 9, 68 ± 11 and 90 ± 10 mb at $E_{\text{lab}} = 83$, 88, 93, 98 and 103 MeV, respectively. The possible CF contribution to Lu, Yb, Tm and Ho isotopes constitute up to a maximum value of 1% of these extracted ICF cross-sections. ICF cross-section extracted in this way would depend upon parameters of PACE2 calculations. However, as parameters of PACE2 code are fixed using the cross-sections of W isotopes, which constitute about 86–93% of the total fusion cross-section, model calculations are not expected to add any significant uncertainty on extracted ICF cross-sections. Further, any variation in the model parameters would not be able to reproduce substantial cross-section of ERs formed in large mass transfer channels such as those of Lu, Yb, Tm and Ho isotopes. Statistical model calculations using nuclear reaction video (NRV) code available at *http://nrv.jinr.ru\nrv*[41–44] also gave similar estimate of incomplete fusion cross-sections.

Wilczynski *et al.*[1,16] proposed sum-rule model to explain the cross-section for incomplete fusion channels as well as complete fusion channel. Within the framework of sum-rule model, various incomplete fusion channels are localized in successive angular momentum windows beyond critical angular momentum for complete fusion "$l_{\text{cr}}(\text{CF})$". According to this model the cross-section for a particular channel is given by

$$\sigma(i) = \pi \,\lambdabar^2 \sum_{l=0}^{l_{\text{max}}} (2l+1) \frac{T_l(i)p(i)}{\sum_j T_l(j)p(j)} \tag{3}$$

where, $\lambdabar = \hbar/\sqrt{2\mu E}$ is the reduced wavelength at energy E and μ is reduced mass, $p(i)$ and $T_l(i)$ are the probability and transmission coefficient for the ith reaction channel respectively. $T_l(i)$ is given as

$$T_l(i) = \left[1 + \exp\left(\frac{l - l_{\text{lim}}(i)}{\Delta} \right) \right]^{-1} \tag{4}$$

where, $l_{\text{lim}}(i)$ is the limiting angular momentum in the entrance channel for the reaction channel i and is equal to $(A_P/n)l_{\text{cr}}(i)$. A_P is the projectile mass number, n is the number of transferred nucleons and $l_{\text{cr}}(i)$ is the critical angular momentum at which the pocket in the entrance channel potential vanishes for the reaction channel i. The parameter Δ is the diffuseness of the l-distribution. The probability $p(i)$ for a reaction channel i is given as[45]

$$P(i)\alpha \exp((Q_{gg}(i) - Q_c(i))/T) \tag{5}$$

where, $Q_{gg}(i)$ is the ground state Q values for the reaction channel i and $Q_c(i)$ is the difference between exit and entrance channel Coulomb energy calculated at inter-nuclear separation distance $R(A_P^{1/3} + A_T^{1/3})$ and T is the temperature in the interaction region.[1] Wilczynski *et al.* used $T = 3.5$ MeV, $R = 1.55$ Fm and $\Delta = 1.7\ \hbar$ in the calculation of cross-sections for different channels in ^{14}N $+$ ^{159}Tb at $E_{\text{lab}} = 140$ MeV.[1] Results of sum-rule model calculations with these parameters for ^{19}F $+$ ^{159}Tb reaction are shown as a function of Z_{PLF} in Figs. 3(a)–(e) (solid lines), where Z_{PLF} is the Z of the outgoing PLF ($= Z_{\text{projectile}} + Z_{\text{Target}} - Z_{\text{ERs}}$). The cross-sections for different isotopes for a given Z have been combined. For comparison, experimental cross-sections of ERs (after apportioning the CF and ICF contributions using the calculations of PACE2) corresponding to the emission of PLFs with different Z are also shown in this figure. It can be seen from this figure that the cross-sections for ERs formed in incomplete fusion channels are underestimated by sum-rule model and the difference is beyond any possible uncertainty due to the model calculations. Cross-section of some of the ERs could not be measured due to their unsuitable decay characteristic or large contribution from precursors. However, inclusion of cross-section of these ERs will further increase the discrepancy between experimental cross-sections and sum-rule model[1,16] calculations. The difference between sum-rule calculations and experimental cross-sections increases with decreasing beam energy. A better agreement between sum-rule model calculations and experimental data, as judged by the chi square, can be obtained by increasing the value of temperature parameter. However, this requires the value of parameter T to be around 6 MeV, which seems to be high for the beam energy range of the present study. Also, significant difference between calculated and experimental cross-section exists for heavier PLFs. As pointed out in earlier studies[6,7] underestimation of experimental ICF cross-section by sum-rule model at lower beam energies (<10 MeV/nucleon) is due to the strong preference for complete fusion for collision trajectories with $l < l_{\text{cr}}(\text{CF})$. At lower beam energies, maximum angular momentum l_{max} populated in the reaction is lower or close to $l_{\text{cr}}(\text{CF})$. Therefore, sum-rule model predicts small cross-section for incomplete fusion at these beam energies. However, significant cross-sections for ICF have been observed at lower beam energies (<10 MeV/nucleon) in several studies.[19,20,24,25,29,30,33,34] This observation suggests the contribution to ICF from collision trajectories with $l < l_{\text{cr}}(\text{CF})$.

In a recent work,[7] calculation of transmission coefficient in the sum-rule model was modified to allow effective competition from ICF for collision trajectories with $l < l_{\text{cr}}(\text{CF})$. The modified transmission coefficient $T'_l(i)$ is calculated using the equation

$$T'_l(i) = \left[1 + \exp\left(\frac{l - l_{\text{lim}}(i)}{\Delta} \right) \right]^{-1} (e^{nl\,F_T})^{-1}, \qquad (6)$$

where, n is the number of transferred nucleons and the parameter F_T governs how rapidly the transmission coefficient will decrease with increasing l. The term $(e^{nl\,F_T})^{-1}$ decreases the transmission coefficient with increasing number of trans-
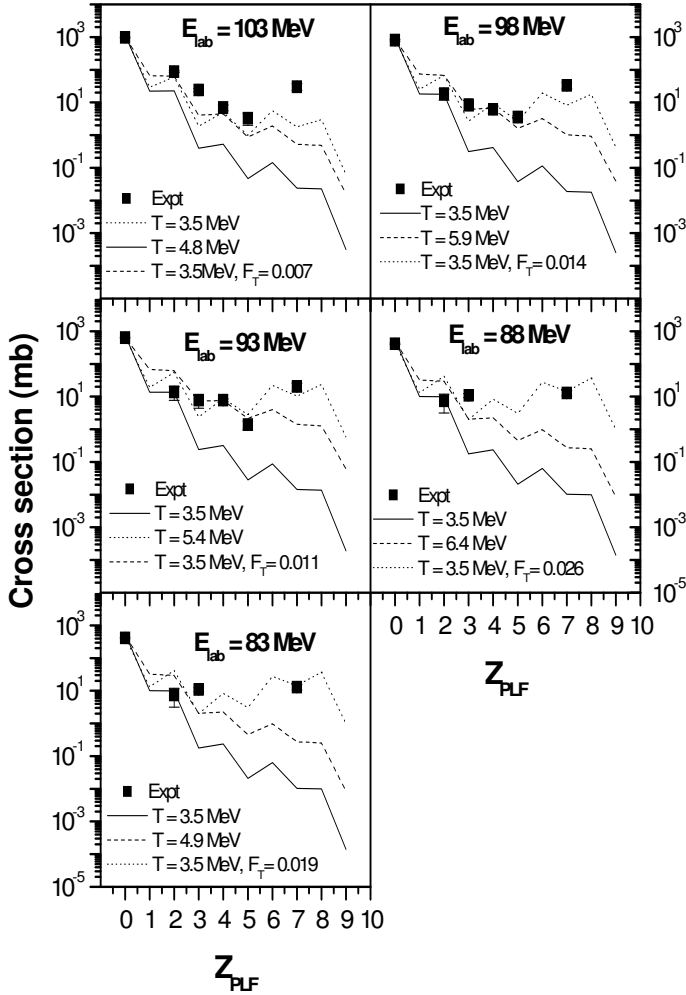
Fig. 3. Plot of experimental evaporation residue (ER) cross-sections as a function of Z_{PLF} of the corresponding channel, at $E_{\mathrm{lab}} = 83, 88, 93, 98$ and 103 MeV, where $Z_{\mathrm{PLF}} = Z_{\mathrm{projectile}} + Z_{\mathrm{Target}} - Z_{\mathrm{ERs}}$. Results of sum-rule model calculation[1,2] and modified sum-rule model calculation are also shown in the figure. Solid lines are sum-rule model calculation with $T = 3.5$ MeV. Dashed lines are sum-rule model calculation with T as free parameter. Dotted lines are modified sum-rule model calculations[7] with $T = 3.5$ MeV and F_T as a free parameter.

ferred nucleons and, thus, reduces the strong preference for complete fusion for collision trajectories with $l < l_{\mathrm{cr}}(\mathrm{CF})$. Cross-sections of PLFs calculated with modified sum-rule model with F_T as free parameter are shown as dotted lines in Figs. 3(a)–(e). In this calculations T was fixed at 3.5 MeV as number of data points were not enough, particularly at lower beam energies, to constrain the fit with two parameters. The modified sum-rule model reproduces experimental cross-sections quite well as shown in Figs. 3(a)–(e). Thus, modified sum-rule model, after incorporating

effective competition from ICF below $l_{cr}(CF)$, successfully explains experimental ICF cross-section at lower beam energies.

4. Conclusions

Present measurements of evaporation residue cross-sections by radiochemical method shows a significant contribution from incomplete fusion at lower beam energies (~ 5 MeV/nucleon). This observation suggests that it is necessary to include the contribution to incomplete fusion from collision trajectories with $l < l_{cr}(CF)$ to explain the ICF cross-section in this beam energy domain. Sum-rule model underestimated the ICF cross-section as it strongly favors complete fusion for collision trajectories with $l < l_{cr}(CF)$. Modified sum-rule model calculation, which allows effective competition from incomplete fusion for collision trajectories with $l < l_{cr}(CF)$, was in better agreement with the experimental data.

Acknowledgment

References

1. J. Wilczynski, K. Siwek-Wilczynska, J. Van Driel, S. Gonggrijp, D. C. J. M. Hageman, R. V. F. Janssens, J. Lukasiak, R. H. Siemssen and S. Y. Van Der Werf, *Nucl. Phys. A* **373** (1982) 109.
2. H. C. Britt and A. R. Quinton, *Phys. Rev.* **124** (1964) 877.
3. J. Galin, B. Gatty, D. Guirean, C. Rousset, V. C. Schlotthauer-Voos and X. Tarrago, *Phys. Rev. C* **9** (1974) 1126.
4. B. S. Tomar, A. Goswami, G. K. Gubbi, A. V. R. Reddy, S. B. Manohar, B. John and S. K. Kataria, *Phys. Rev. C* **58** (1998) 3478.
5. S. Sodaye, K. Sudarshan, B. S. Tomar, A. Goswami, S. Mukherjee and K. Mahata, *Eur. Phys. J. A* **14** (2002) 371.
6. R. Tripathi, K. Sudarshan, S. Sodaye and A. Goswami, *J. Phys. G* **35** (2008) 025101.
7. R. Tripathi, K. Sudarshan, S. Sodaye, A. V. R. Reddy, A. Goswami, B. K. Nayak and S. K. Sharma, *Phys. Rev. C* **79** (2009) 064604.
8. C. Gerschel, *Nucl. Phys. A* **387** (1982) 297c.
9. T. Inamura, A. C. Kahler, D. R. Zolnowski, U. Garg, T. T. Sugihara and M. Wakai, *Phys. Rev. C* **32** (1985) 1539.
10. K. Sudarshan, S. Sodaye, K. Surendra Babu, S. Mukherjee, S. K. Rathi, K. Mahata, A. Goswami and B. S. Tomar, *Phys. Rev. C* **69** (2004) 027603.
11. P. P. Singh *et al.*, *Phys. Lett. B* **671** (2009) 20.
12. T. Udagawa and T. Tamura, *Phys. Rev. Lett.* **45** (1980) 1311.
13. J. P. Bondorf, J. N. Dey, G. Fai, A. O. T. Karvinen and J. Randrup, *Nucl. Phys. A* **333** (1980) 285.
14. M. Blann, *Phys. Rev. C* **31** (1985) 1245.
15. V. I. Zagrebaev, *Ann. Phys. (N.Y.)* **197** (1990) 33.
16. K. Siwek-Wilczynska, E. H. du Marchie van Voorthuysen, J. van Popta, R. H. Siemssen and J. Wilczynski, *Phys. Rev. Lett.* **42** (1979) 1599.

17. H. Morgenstern, W. Bohne, W. Galster, K. Grabisch and A. Kyanowski, *Phys. Rev. Lett.* **52** (1984) 1104.

18. H. Morgenstern, W. Bohne, W. Galster and K. Grabisch, *Z. Phys. A* **324** (1986) 443.

19. K. Surendra Babu, R. Tripathi, K. Sudarshan, S. Sodaye, A. Goswami, B. D. Shrivastava and B. S. Tomar, *Nucl. Phys. A* **739** (2004) 229.

20. K. Surendra Babu, R. Tripathi, K. Sudarshan, B. D. Shrivastava, A. Goswami and B. S. Tomar, *J. Phys. G: Nucl. Part. Phys.* **29** (2003) 1011.

21. B. Becker *et al.*, *Eur. Phys. J. A* **18** (2003) 639.

22. M. Cavinato, E. Fabrici, E. Gadioli, E. E. Gadioli, P. Vergani, M. Crippa, G. Colombo, I. Redaelli and M. Ripamonti, *Phys. Rev. C* **52** (1995) 2577.

23. C. Birattari *et al.*, *Phys. Rev. C* **54** (1996) 3051.

24. S. Gupta, B. P. Singh, M. M. Musthafa, H. D. Bhardwaj and R. Prasad, *Phys. Rev. C* **61** (2000) 064613.

25. B. B. Kumar, A. Sharma, S. Mukherjee, S. Chakrabarty, P. K. Pujari, B. S. Tomar, A. Goswami and S. B. Manohar, *Phys. Rev. C* **59** (1999) 2923.

26. L. J. Mudau *et al.*, *Nucl. Phys. A* **761** (2005) 190.

27. E. Z. Buthelezi, F. Cerutti, E. Gadioli, G. F. Steyn, A. Pepe, S. H. Connell and A. A. Cowley, *Eur. Phys. J. A* **28** (2006) 193.

28. E. Z. Buthelezi, F. Cerutti, E. Gadioli, G. F. Steyna, S. H. Connell and A. A. Cowley, *Nucl. Phys. A* **753** (2005) 29.

29. A. Sharma, B. Bindu Kumar, S. Mukherjee, S. Chakrabarty, B. S. Tomar, A. Goswami and S. B. Manohar, *J. Phys. G* **25** (1999) 2289.

30. M. K. Sharma, Unnati, B. K. Sharma, B. P. Singh, H. D. Bhardwaj, R. Kumar, K. S. Golda and R. Prasad, *Phys. Rev. C* **70** (2004) 044606.

31. E. Gadioli *et al.*, *Nucl. Phys. A* **708** (2002) 391.

32. E. Gadioli *et al.*, *Eur. Phys. J. A* **17** (2003) 195.

33. R. Tripathi, K. Sudarshan, S. Sodaye, S. K. Sharma, A. V. R. Reddy and A. Goswami, *Eur. Phys. J. A* **42** (2009) 25.

34. R. Ali, D. Singh, M. A. Ansari, M. H. Rashid, R. Guin and S. K. Das, *J. Phys. G* **37** (2010) 115101.

35. V. Zagrebaev and W. Greiner, *J. Phys. G* **34** (2007) 1.

36. A. Gavron, *Phys. Rev. C* **21** (1980) 230.

37. R. B. Firestone and V. S. Shirley, *Table of Isotopes*, 8th edn. (Wiley-interscience Publication, New York, 1999).

38. P. K. Mukhopadhyaya, in *Proc. DAE Symposium on Intelligent Nuclear Instrumentation*, Mumbai, 2001, p. 307.

39. S. K. Kataria, V. S. Ramamoorthy and S. S. Kapoor, *Phys. Rev. C* **18** (1978) 549.

40. C. H. Dasso and S. Landowne, *Comput. Phys. Commun.* **46** (1987) 187.

41. A. V. Ignatyuk *et al.*, *Sov. J. Nucl. Phys.* **21** (1975) 612; A. V. Ignatyuk *et al.*, *Sov. J. Nucl. Phys.* **21** (1975) 225.

42. V. I. Zargebaev *et al.*, *Phys. Rev. C* **65** (2001) 014607.

43. A. V. Ignatyuk, *The Statistical Properties of the Excited Atomic Nuclei* (Energoatomizdat, Moscow, 1983).

44. A. R. Junghans *et al.*, *Nucl. Phys. A* **629** (1998) 635.

45. J. P. Bondorf, F. Dickmann, D. H. E. Gross and P. J. Siemens, *J. de Phys. Colloq.* **32** (1971) C6–145.